ADVANCING EARTH AND SPACE SCIENCE

Water Resources Research

RESEARCH ARTICLE

10.1029/2021WR031212

Seasonal and Longitudinal Variations in Suspended Load Connectivity Between River Channels and Their Margins

C. E. Renshaw[1], E. N. Dethier[1], J. D. Landis[1], and J. M. Kaste[2]

[1]Department of Earth Sciences, Dartmouth College, Hanover, NH, USA, [2]Geology Department, William & Mary, Williamsburg, VA, USA

Key Points:

- We observe seasonal variations in the ratio of suspended load exported from the watershed versus stored in channel margins
- Greater fractional area of deposition along margins of headwaters facilitates trapping of suspended load that limits suspended load export
- Increasing transport length with increasing watershed area systematically decouples the channel from terrestrial organic exchange

Supporting Information:

Supporting Information may be found in the online version of this article.

Correspondence to:

C. E. Renshaw,
carl.renshaw@dartmouth.edu

Citation:

Renshaw, C. E., Dethier, E. N., Landis, J. D., & Kaste, J. M. (2022). Seasonal and longitudinal variations in suspended load connectivity between river channels and their margins. *Water Resources Research*, *58*, e2021WR031212. https://doi.org/10.1029/2021WR031212

Received 10 SEP 2021
Accepted 21 MAR 2022

Author Contributions:

Conceptualization: E. N. Dethier
Formal analysis: J. D. Landis
Investigation: E. N. Dethier
Methodology: E. N. Dethier, J. D. Landis
Writing – review & editing: E. N. Dethier, J. D. Landis, J. M. Kaste

Abstract

Input of organic matter into stream channels is the primary energy source for headwater ecosystems and ultimately carbon to the oceans and hence is an important component of the global carbon cycle. Here, we quantify organic-rich fine sediment mobilization, transport, and storage in a Strahler fourth-order stream during individual intermediate-sized storm events. By combining measurements of fallout radionuclides (FRNs) ^{7}Be and ^{210}Pb and stable water isotopes with a conceptual model of suspended load trapping by channel margins, we find that the channel bed was consistently a source of suspended load to the channel margins. Relative to storage on the channel margins, suspended load export increased through the spring and summer, perhaps related to the in-channel decomposition of organic debris as indicated by its FRN exposure age and changing bulk δ^{13}C composition. Trapping of suspended load by riparian margins limits sediment transport distances, which, given sufficient discharge to fully suspend the load, is nearly independent of stream discharge for sub-bankfull discharges. Limited data indicate that the fractional size of the channel margins where trapping occurs decreases with increasing watershed area. Increasing transport length and decreasing fractional margin area with increasing watershed area results in a systematic downstream decoupling of the channel from local terrestrial organic matter exchange. These findings provide a framework for understanding suspended load dynamics in formerly glaciated regions where sediment production and fluxes are generally low and thus the annual input of organic debris is a major component of suspended load budget.

Plain Language Summary

The decomposition of organic-rich debris (leaves, twigs, etc.) within stream channels serves as an important organic carbon source to stream margins or banks. During moderate storm events, we observed that the channel bed was consistently a source of organic-rich suspended load that is then trapped by the channel margins. Through spring and summer less of the suspended load is trapped by the margins, increasing the fraction of the suspended load exported. This decreased trapping and increased export may be related to changes in the character of the suspended load due to the in-channel decomposition of organic debris. Trapping of suspended load by channel margins limits the transport distance of suspended load, systematically decoupling the channel from the channel margins with increasing watershed size. These findings provide a framework for understanding suspended load transport in formerly glaciated regions where the annual input of organic debris is a significant component of suspended load budget.

1. Introduction

Input of particulate organic matter (e.g., sticks and leaves) both directly to the channel and as runoff from the surrounding hillslopes is the primary energy source for headwater ecosystems (Fisher & Likens, 1972, 1973; Webster et al., 1995). After introduction to the channel, particulate organic matter is broken down by physical and biological processes into successively smaller size fractions (Cummins, 1975) and ultimately nearly half of it is metabolized or photolyzed and returned to the atmosphere as CO_2 (Aufdenkampe et al., 2011). The remaining, unrespired carbon is transported from the watershed and about two-thirds of it delivered to the oceans. Hence, fluvial systems are an important component of the global carbon cycle (Galy et al., 2015; Wohl et al., 2012). Along this pathway, the uptake of atmospheric contaminants such as Hg by foliage and their subsequent deposition to stream via litterfall is an important input of atmospheric contaminants to riparian ecosystems (Wang et al., 2016). The transport and fate of particulate organic matter and fine, organic-rich sediment thus also plays a vital role in transport of both nutrients and pollutants, and the degradation of downstream channel, reservoir, and estuary habitats (Carter et al., 2006; Chartin et al., 2013; Gibbs, 1973; Horowitz, 1995; Landis et al., 2012a; Le Gall et al., 2017; MacDonald & Coe, 2007; Vorosmarty et al., 2003; Walling, 2013; Whiting et al., 2005).

However, the time scales of organic-rich fine suspended load transport in headwater streams, and the linkages from headwater to downstream systems are complex and need further characterization.

The active channel and its margins can be a significant source or sink of fine-grained, organic-rich sediment (Skalak & Pizzuto, 2010). Although initially assumed to move rapidly downstream as washload (Garcia, 2007), fine-grained sediment is now recognized to move in a series of discrete steps (Bilby & Likens, 1980; Bonniwell et al., 1999) separated by periods of storage on channel margins that can approach 10^3 years for coarse suspended load (Pizzuto et al., 2014). Here, the channel margins are defined as those parts of the bankfull channel below the floodplain where fine sediment can collect. By this definition, channel margin areas include, but are not restricted to, the edges of the channel between the water's edge and the floodplain. Importantly, however, channel margin areas also include in-channel areas where fine sediment can collect, such as behind debris dams and large woody debris (Bilby & Likens, 1980; Skalak & Pizzuto, 2010). Subsequently, we refer to any fine sediment deposited within the channel as channel margin deposits. Wallace et al. (1995) observed that most coarse particulate organic matter was exported during the largest storms, suggesting significant sediment trapping and storage during small to moderate events. Indeed, Underwood et al. (2015) demonstrated that as much as 90% of the suspended load mobilized during small to intermediate storm events was trapped by the channel margins. Similarly, Skalak and Pizzuto (2010) found that in the partly confined, mixed bedrock-alluvial South River (Virginia, USA), in-channel fine-grained margin deposits store 20–40% of the annual suspended load.

Despite these previous studies, understanding of the processes that control the transport and storage of fine sediment remains a challenge. This information is important for understanding linkages between upland sediment sources and downstream sediment delivery (Fryirs, 2013), the transport of particle bound contaminants (Pizzuto, 2020), and for predicting how fine sediment transport may change in response to changing climate. To help address this gap in understanding, here, we take advantage of a recently developed methodology that combines measurements of the mass balances of the fallout radionuclides (FRNs) ^{7}Be and ^{210}Pb and the stable isotopes of hydrogen in water to quantify fine sediment transport and fate during individual storm events (Underwood et al., 2015). We focus on small to intermediate storms because they, on average, transport the largest portion of the total sediment load (Wolman & Miller, 1960). Also, while some fine-grained channel margin deposits have storage time scales of over 70 years (Skalak & Pizzuto, 2010), most in-channel organic-rich fine sediment is typically assumed to exchange annually (Gellis et al., 2017), dampening the impact of bankfull or greater discharges with recurrence intervals longer than 1 year on suspended load transport. We constrain the exposure age of the suspended load using the different decay rates of two FRNs (Landis et al., 2014) and, as a qualitative indication of the evolving character of suspended load, compare these ages to the bulk δ^{13}C composition of the sediment. Finally, we develop a conceptual model of suspended load trapping by channel margins to quantify the fractional size of the channel margins and the characteristic suspended load transport lengths. In so doing we seek to determine the impact of discharge and seasonality on the fraction of suspended load exported from the watershed, the size of the channel margins, and the characteristic suspended load transport length. We demonstrate the application of this model using two different data sets, first based on an isotopic mass balance and the second based on measured transects of suspended load concentrations.

2. Background and Theory

2.1. Fractional Margin Area and Characteristic Transport Length

The equation of mass balance of suspended load in the channel can be written (Pizzuto, 1987)

$$\frac{\partial \xi'}{\partial t} - \varepsilon_y \frac{\partial^2 \xi'}{\partial y^2} = ER' - DR' \tag{1}$$

where ε_y [$L^2\,T^{-1}$] is the transverse diffusivity, y [L] is the cross-channel coordinate, t [T] is time, ER [$M\,L^{-2}\,T^{-1}$] and DR [$M\,L^{-2}\,T^{-1}$] are the erosion and deposition rates at the bed, and the vertically integrated suspended load mass ξ' [$M\,L^{-2}$] is defined as

$$\xi'(y,t) = \int_0^{h'(y,t)} c'(y,z,t)\,dz \tag{2}$$

10.1029/2021WR031212

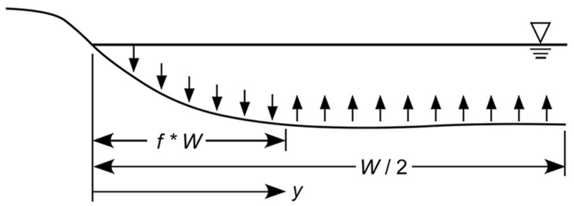

Figure 1. Conceptual model of channel with a lateral depositional zone that is some fraction *f* of the event-averaged channel width *W*. The channel geometry is assumed symmetric. Note that, especially in the headwaters, marginal areas are not limited to the lateral edges. See text for details.

where c $[M\,L^{-3}]$ is the suspended load concentration, h $[L]$ is the flow depth, and the prime indicates time-dependent values. To simplify the analyses, we assume that event-averaged values can be used to approximate the time-averaged steady-state mass balance during a moderate discharge event, allowing the above equations to be simplified as (Parker, 1978)

$$-\varepsilon_y \frac{d^2\xi}{dy^2} = ER - DR \tag{3}$$

$$\xi(y) = \int_0^{h(y)} c(y,z)\,dz \tag{4}$$

Underwood et al. (2015) showed that during moderate discharge events ($0.07 < Q_{peak}/Q_2 < 0.36$, where Q_{peak} and Q_2 are the event peak and 2-year recurrence discharges) in a small (~15 km^2), undeveloped, gravel-bedded tributary of the Connecticut River (USA), the mass of sediment deposited onto the channel margins accounts for as much as 90% of the sediment mobilized from the bed, with the remainder of the mobilized sediment exported downstream as suspended load. While sediment undoubtedly exchanges in both directions, the net transfer of sediment from the channel to the margins indicates that, in simplest terms, the channel cross section can be partitioned into two regions, an erosional region in the central channel and a depositional region in the channel margins. As noted earlier, especially in headwater systems, the depositional margins may also include in-channel areas where fine sediment collects such as behind debris dams (Bilby & Likens, 1980; Skalak & Pizzuto, 2010). However, to simplify the analysis, we conceptualize the stream as a central thalweg region where erosion dominates and a depositional region along the lateral edges (Figure 1). The key idea is the fractional size *f* of the margin areas with respect to the event-averaged channel width and not the specific distribution of the marginal areas.

Phenomenologically, we suggest that the erosional region is defined by that part of the channel where the rate of fine-particle suspension from the bed exceeds the rate of particle deposition. Hamm et al. (2011) showed that the rates of fine-particle deposition in an open channel flow approached Stokes' settling velocity in slow flows but diminished systematically with increasing mean flow speed. The reduction in effective particle settling velocity with increasing flow velocity was independent of suspended silt-particle size and bed porosity. They interpreted the reduction in particle deposition to the effects of Saffman lift in the linear shear flow near the bed boundary that exceeded the submerged weight of the particles (Nino et al., 2003; Saffman, 1965). Hamm et al. (2009) showed that the Saffman lift criterion could be used to quantify the effective settling rate for silt particles as large as 0.04 mm, with Clark (2017) later extending the range of this criterion to very fine sand particles as large as 0.15 mm. Hamm et al. (2011) summarized the effective settling velocity of silts and very fine sands as a function of the normalized mean flow velocity U_+, [–] defined as

$$U_+ = \frac{\bar{u}}{(\nu g R)^{1/3}} \tag{5}$$

where $\bar{u}$ $[L\,T^{-1}]$ is the mean channel flow velocity, ν $[L^2\,T^{-1}]$ is the kinematic viscosity, g $[L\,T^{-2}]$ is the gravitation acceleration, and R [–] is relative excess density $(\rho_s - \rho_f)/\rho_f$, where ρ_s and ρ_f are the solid and fluid densities $[M\,L^{-3}]$. Their experimental observations showed that for values of $U_+ > \sim 27$ the effective settling velocity is near zero and, therefore, silt and very fine sand-sized particles stay in suspension. This dimensionless threshold corresponds to a mean flow velocity $\bar{u} \sim 0.68$ m/s for particles with a density of quartz (2.65 g/cm^3). Suspended load is typically composed of mineral and organic components bound to each other via sorption, flocculation, aggregation, and other mechanisms (Droppo, 2001; Rose et al., 2018) and thus the particles have an average density less than that of quartz. For characteristic densities of organic-rich particles in the range of 1.2–1.5 g/cm^3, the threshold flow velocity for net particle suspension is 0.3–0.4 m/s.

We assume that once particles are suspended, turbulence fully mixes the suspended load, resulting in a nearly constant suspended load concentration across the channel except very near the edges (in the absence of in-channel depositional areas). As shown in Figure 2a, this assumption is consistent with, e.g., the field observations of Hubbell and Matejka (1959). Thus, if the channel depth is approximately uniform in the central erosional region of the channel, then the depth-integrated suspended load mass is constant, i.e.,

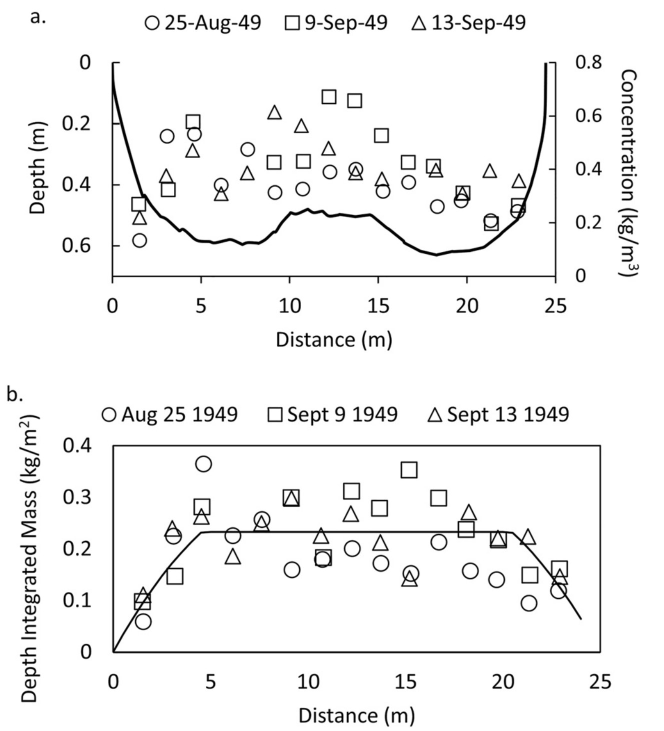

Figure 2. Lateral profiles of (a) average depth (solid line) and vertically averaged suspended load concentration (points) and (b) best fit of Equations 6 and 9 (line) to measurements of depth-integrated suspended load mass (points) in section C, Middle Loup River (data from Hubbell and Matejka (1959)).

$$\xi(y) = \xi_c \quad fW < y < W(1-f) \tag{6}$$

where the width of the lateral depositional zone is some fraction f [–] of the event-averaged channel width W [L] (Figure 1).

In contrast to the nearly uniform depth-integrated suspended load mass in the erosional region of the channel, ξ decreases across the lateral edges of the channel due to both decreased flow depth and decreased suspended load concentration due to deposition. As shown in Figure 2b, this assumption also is consistent with, e.g., the field observations of Hubbell and Matejka (1959). While for the simplified geometry in Figure 1, the rate of deposition varies across the lateral region, approaching the settling velocity as $U_+ \to \sim 5$ or for typical organic-rich particle densities, $\bar{u} \to \sim 0.1$ m/s (Hamm et al., 2011), this variation depends on the details of the channel geometry and flow velocities that are difficult to generalize, especially in the case where marginal areas are not restricted to the lateral edges. Instead, here, we approximate the deposition rate as uniform across all channel margin areas and related to the event-averaged total margin deposition rate per unit downstream distance Q_{ss}^{margin} [$M\ T^{-1}\ L^{-1}$]. Thus, the mass balance on the channel margins can be written

$$\varepsilon_y \frac{d^2\xi}{dy^2} = \frac{Q_{ss}^{margin}}{2fW} \quad y < fW \tag{7}$$

where the factor of two arises because deposition occurs on both lateral margins in Figure 1. Since the simplified channel is assumed symmetric, we limit our attention to the margin nearest the coordinate origin. The flux into this lateral margin at its boundary with the central erosional region must match the event-averaged deposition rate

$$-\varepsilon_y \frac{d\xi}{dy}\Big|_{y=fW} = \frac{Q_{ss}^{margin}}{2} \tag{8a}$$

And since the flow depth is zero at the channel edge

$$\xi(y=0) = 0 \tag{8b}$$

Integrating Equation 7 subject to the two boundary conditions (Equation 8) yields

$$\xi(y) = \frac{Q_{ss}^{margin}}{\varepsilon_y}\left(\frac{y^2}{4fW} - y\right) \quad y < fW \tag{9}$$

Figure 2b shows a least-squares best fit of Equations 6 and 9 to the measurements of the lateral distribution of depth-integrated suspended load concentrations of the Middle Loup River near Dunning, Nebraska (Hubbell & Matejka, 1959). Note that there are two free parameters in Equation 9, the fractional size of the lateral margins f and the ratio $Q_{ss}^{margin}/\varepsilon_y$. Using Equation 9 to solve for the depth-integrated sediment mass at the boundary between the lateral margin and the erosional region

$$\xi(y=fW) = \xi_c = -\frac{3fWQ_{ss}^{margin}}{4\varepsilon_y} \tag{10}$$

Shows that $Q_{ss}^{margin}/\varepsilon_y$ is a function of ξ_c and hence the latter can also be used as the second free parameter. The least-squares best fit values for these parameters to the Middle Loup River data are $\xi_c = 0.23 \pm 0.01$ kg/m^2 and $f = 0.18 \pm 0.03$. Thus, the depositional region occupies one-third of the channel ($2f$).

In using Equation 10, we assume $\xi_c = HC$, where H [L] and C [$M\ L^{-3}$] are storm average flow depth and suspended load concentration. Empirically, diffusivities of channel flow are often observed to follow relationships of the form

10.1029/2021WR031212

$$\varepsilon_y = ahu_* \tag{11}$$

where $u_* = \sqrt{ghS}$ is the friction velocity [$L\ T^{-1}$], where S [–] is the channel slope, and a [–] is a constant that depends on the flow geometry and is typically in the range 0.077–0.13 (Engelund, 1970; Parker, 1978). In calculating the friction velocity, we assume the flow depth in the channel margins is $h = H/2$ and, since turbulence may not be fully developed in the margins, take the low-end value for a.

The channel geometry and vertically averaged suspended load concentrations for the Middle Loup River are shown in Figure 2a. The suspended load concentrations are similar across the channel, indicating the channel is generally well mixed. Thus, the residence time of suspended load in the channel can be approximated as the reservoir residence time, defined as

$$t_{mix} = -\frac{CWH}{Q_{ss}^{margin}} \tag{12}$$

where C and H are the event-averaged suspended load concentration and flow depth, respectively. If the flow velocity V_w [$L\ T^{-1}$] is approximately constant, the residence time can be expressed as a characteristic suspended load transport length L [L]

$$L = V_w t_{mix} = -\frac{V_w CWH}{Q_{ss}^{margin}} \tag{13}$$

The above analyses provide a quantitative framework for assessing the impact of seasonality and discharge on suspended load transport. Specifically, during small to intermediate storm events ($Q_{peak} < Q_2$) we seek to determine the impact of discharge and seasonality on the ratio of suspended load deposited on the channel margins to that exported out of the watershed $Q_{ss}^{margin}/Q_{ss}^{stream}$, the fractional size of the channel margins f, and the characteristic suspended load transport length L. Achieving these objectives requires the quantification of the margin deposition rate per unit downstream distance Q_{ss}^{margin}.

2.2. Quantifying Margin Deposition Rate

FRN tracers have been increasingly used to quantify sediment mobilization and storage within catchments (Porto et al., 2013; Renshaw et al., 2014; Walling et al., 2009; Zhang et al., 2006), but much of this earlier work is limited to integrating longer-term average sediment movement. Recently, Underwood et al. (2015) demonstrated an alternative extension of the FRN tracer approach to quantify lateral exchanges during individual storm events by using a joint isotopic mass balance approach for the short-lived radionuclide ^{7}Be and the stable isotopes of water (^{2}H). Rather than allowing for detailed spatial analysis of sediment exchange across the channel margins, this approach quantifies the integrated net exchange occurring along all channel margins upstream of the sampling location. The approach is limited to discharges less than bankfull (i.e., discharges with a recurrence interval <~1.5–2 years) where increases in discharge result primarily from direct precipitation on the stream surface, not surface runoff (Gomi et al., 2002; Renshaw et al., 2003), and the primary sources of sediment to the stream are limited to the channel bed and channel margins. While discharges during these storms are not sufficient to inundate channel floodplains, they are still thought to, on average, transport the largest portion of the total sediment load (Wolman & Miller, 1960). Because the channel margins are partially inundated as discharge increases, they can either sequester or supply sediment in response to changing discharge. Any overland flow that occurs during these intermediate storms is expected to be restricted to near-channel regions. Thus, the upland reaches of the watershed, i.e., those areas outside the channel and its immediate margins, are unlikely to be a significant source of sediment during these storms (Hornbeck, 1973).

In this approach, the net transfer of material between the stream and channel margins and beds is quantified using the mass balance for the suspended load flux in the stream Q_{ss}^{stream}, yielding

$$Q_{ss}^{stream} = Q_{ss}^{bed} + Q_{ss}^{margin} \tag{14}$$

where Q_{ss}^{margin} and Q_{ss}^{bed} are the net transfer of sediment to the stream from the margins and channel bed, respectively. A negative flux indicates that the dominant flux direction is out of the stream and onto either to the margins

10.1029/2021WR031212

or the bed (depositional), while a positive flux indicates that the dominant direction of flux is into the stream from either the margins or the bed (erosional).

Assuming no input from upland soil source, combining Equation 14 with the isotopic mass balance, the flux of suspended load coming from channel margins can be written (Underwood et al., 2015)

$$Q_{ss}^{margin} = \frac{Q^{stream}\,\alpha_{Be}^{stream} - Q_{ss}^{stream}\,\alpha_{Be}^{stream} - Q^{precip}\,\alpha_{Be}^{precip}}{\alpha_{Be}^{margin\,or\,stream} - \alpha_{Be}^{bed}} \tag{15}$$

where α_{Be}^{stream} [Bq T^{-1}] and α_{Be}^{bed} represent the ^{7}Be activity of the suspended load in the stream and the material eroding from the channel bed, α_{Be}^{stream} and α_{Be}^{precip} represent the ^{7}Be activity of the stream and precipitation water, and Q^{stream} and Q^{precip} represent the total stream discharge and that due to precipitation. While sediment exchange between the margins and the stream undoubtedly occurs in both directions, we assume that one direction of exchange dominates. Thus the term $\alpha_{Be}^{margin\,or\,stream}$ indicates that either the ^{7}Be activity of the margin sediment α_{Be}^{margin} or the stream α_{Be}^{stream} is used depending on whether the dominant flux is from the margin-to-the-stream (Q_{ss}^{margin} is positive indicating erosion) or stream-to-the-margin (Q_{ss}^{margin} is negative indicating deposition). Using the distinct stable isotopic signatures of pre-event water and precipitation, Q^{precip} can be determined using the isotopic hydrograph separation (Genereux & Hooper, 1998)

$$Q^{precip} = Q^{stream}\left(\frac{\delta D^{stream} - \delta D^{old}}{\delta D^{precip} - \delta D^{old}}\right) \tag{16}$$

where the superscript "*old*" indicates the isotopic composition of water in the watershed prior to the storm (i.e., ground water), the superscript "*precip*" indicates the isotopic composition of precipitation, and the superscript "*stream*" the time varying isotopic composition of stream water during an event. The δD indicates the isotopic ratio, in parts per thousand, of hydrogen's two stable isotopes in water with respect to a reference standard (Vienna-Standard Mean Ocean Water, Kendall & Caldwell, 1998). In practice, all of the radionuclide activities, stable isotopes, total suspended load flux, and stream total discharge and that due to precipitation are readily measured. However, the strong retention of ^{7}Be by organic matter, particularly leaves, implies that the FRN activity of throughfall precipitation under a forest canopy will be less than that of open-fall precipitation. Accordingly, α_{Be}^{precip} in Equation 15 must be an effective activity that accounts for throughfall interception. Here, we do this by collecting throughfall from throughout the catchment and directly measuring its FRN activity. Given the readily measured parameters, the stable isotopes of water are used to solve Equation 16 for Q^{precip}, which is then used in Equation 15 to solve for Q_{ss}^{margin}, which in turn is then used in Equation 14 to solve for Q_{ss}^{bed}. In practice, fluxes are determined for each 15-min interval (based on the frequency of the discharge measurement). The average storm flux is determined by summing the total mass transferred to the margin or bed during and event by the duration of the event.

2.3. Suspended Load Exposure Age and Carbon Isotopic Composition

Although motivated by the joint mass balance for estimating Q_{ss}^{margin}, the measurement of FRN activities also allows for the estimation of suspended load atmospheric exposure age (Landis et al., 2014). Freshly exposed sediment and organic matter will have ^{7}Be to excess ^{210}Pb ratios similar to precipitation (ca. 5–10), while, due to their different rates of radioactive decay, sediment, and organic matter with continuous exposure ages of a year or more have ratios less than ca. 2.

The temporally evolving character of suspended load can be qualitatively evaluated by comparing the atmospheric exposure age of the sediment to its carbon isotopic composition. Feng (2002) showed that the carbon isotopic evolution of decaying organic matter is controlled by substrate quality and microbial growth rate. For leaves and roots, as the high quality (e.g., lipids, amino acids and some carbohydrates) carbon is preferentially consumed, if the low-quality lignin fraction in the organic matter is substantial and its decomposition is sufficiently slow, the bulk δ^{13}C decreases for a period of years before generally increasing once the composition of the organic matter becomes more homogenous. Thus, while difficult to precisely quantify, a decrease in bulk δ^{13}C over time is expected during the preferential decomposition of relatively young ($<\sim$10 years) organic matter and hence bulk δ^{13}C reflects the evolving character of the suspended load as it is preferentially decomposed.

10.1029/2021WR031212

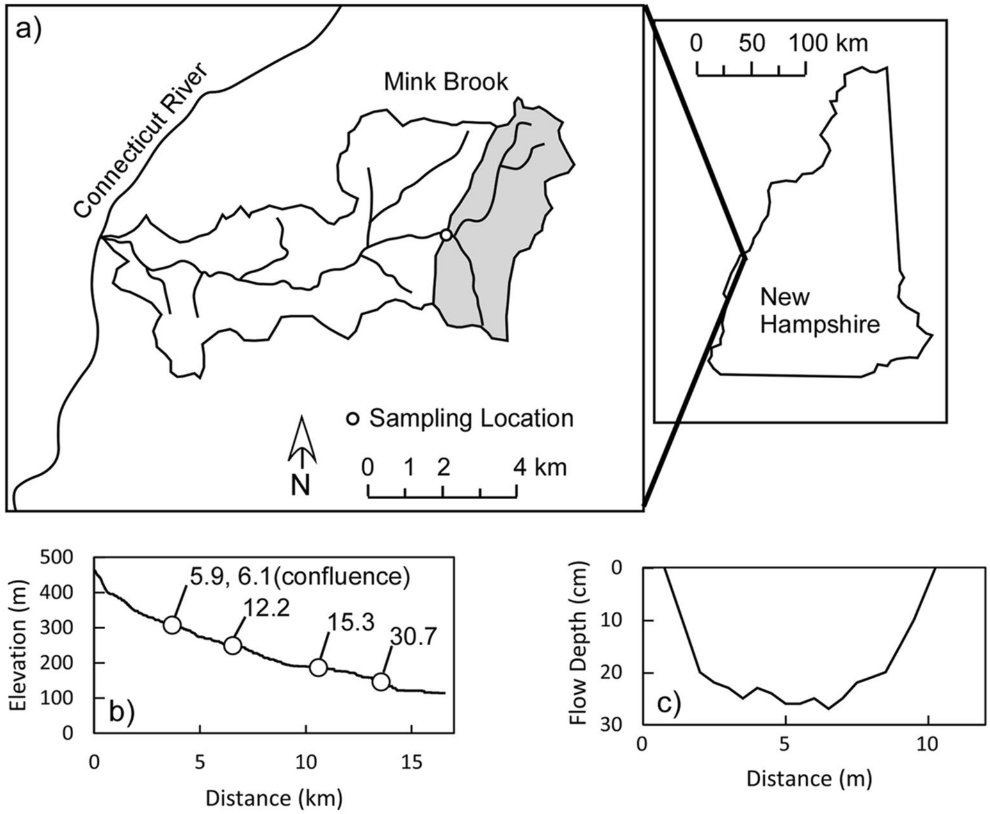

Figure 3. (a) Mink Brook watershed with location of the sampling point highlighted. (b) Long profile with locations of transects and their respective watershed areas (km^2) indicated. The sampling location at the former USGS gage is just downstream of the confluence of the 5.9 and 6.1 km^2 tributaries. (c) Flow depth cross section at sampling site at former USGS gage.

3. Site Description

Here, we apply the methodologies detailed above to determine the impact of discharge and seasonality in channel margin connectivity as quantified by the $Q_{ss}^{margin}/Q_{ss}^{stream}$ ratio, the fractional size of the lateral margins *f*, and the characteristic suspended load transport length *L*. We apply these approaches using data from Mink Brook, a Strahler fourth-order gravel-bedded tributary of the Connecticut River in Hanover, New Hampshire, USA (Figure 3). At the primary sampling area near of former USGS stream gage Mink Brook has a slope of 0.01 and a watershed area of 12 km^2. The long profile with locations of the transects sampled during the large storm (see below) is shown in Figure 3b. Figure 3c shows a cross section of flow depths at the former USGS gage, which is typical of Mink Brook. The channel is partly confined with occasional in-channel bedrock exposures <~30 m in length and generally narrow (a few meters or less) floodplains. The sampling site is in the middle part of the watershed where it is underlain by interstratified metavolcanics and metasediments (Lyons et al., 1997) mantled by 0–2-m thick glacial deposits. Consistent with field observations of its alluvial character, the watershed area at the sampling site is slightly larger than that typically corresponding to the colluvial-alluvial transition (Benda & Dunne, 1997; Brummer & Montgomery, 2003). The upper watershed is primarily undeveloped forested area. Annual precipitation over the watershed averages ~1 m/yr more or less equally distributed throughout the year and with about one-quarter of this falling as snow. Snowmelt runoff produces a reliable spring freshet flood, and frontal systems are responsible for additional high-flow events throughout the year. The median measurable rain event is ~15 mm.

Channel bed and margin areas vary as functions of discharge. Fortunately, the joint isotopic mass balance does not require estimates of the channel bed or margin areas since the volume of new water in the channel is determined from the stable isotopic composition of the discharge. Our methods estimate a mass deposition or erosion rate. A representative area and density are useful for converting the deposited or eroded sediment masses to

10.1029/2021WR031212

Table 1
Summary Characteristics of Sampled Storms

Event date	Precipitation (mm)	Precipitation duration (hr)	Peak Q (m^3/s)	Q/Q_2	Avg SSC (mg/L)	Transport Distance (m)
21 April 2012	24.4	10.25	1.01	0.16	34.04	3059
29 May 2012	24.4	3.25	0.91	0.15	54.02	3151
26 July 2012	33.5	3	0.44	0.07	37.07	3579
8 September 2012	18.0	6.5	0.46	0.07	21.66	4557
8 May 2016	15.7	13.75	2.25	0.36	90.48	4423
14 July 2016	11.0	3.5	0.65	0.11	30.71	3080
20 October 2016	8.2	12.25	0.13	0.02	2.70	53
1 November 2016	32.5	25.25	0.45	0.07	12.51	4454
13 May 2017	39.5	8.25	2.25	0.36	30.56	18,001
3 September 2017	18.1	11.25	0.45	0.07	15.14	7607

an approximate equivalent depth. Based on an estimate of total stream length derived from a watershed digital elevation model and typical stream width, we use 0.05 km^2 as the representative channel area. We further assume a characteristic bulk density of the organic-rich sediment of 1.2 g/cm^3.

4. Methods

4.1. Stream Discharge

Stream stage and turbidity were measured every 15 min at a former United States Geological Survey (USGS) stream gage that was in operation from 1962 to 1997 (gage 01141800). The historical USGS data from this gage were supplemented with data from a stage logger that recorded stream stage every 15 min. Stage was converted to discharge using the USGS rating curve data updated with more recent field discharge measurements. Discharges were normalized by Q_2 (6.17 m^3/s) determined from the available annual peak discharge data collected while the USGS gage was in operation and assuming a log-Pearson distribution (USGS, 1982). For each event, the average discharge was determined over the time required for the discharge to return to its pre-event value. In calculating the transport length (Equation 12), we use the average stream velocity during the event. The average stream velocity was determined by dividing the average discharge by the stream cross sectional area at the former gage at the stage corresponding to the average discharge.

4.2. Event-Based Sampling

Combining our new results with those of Underwood et al. (2015), 6–10 stream samples were taken during each of 10 precipitation events, 5 spanning from spring to late summer 2012, and 5 spanning summer 2016 to summer 2017 (Table 1). These storms varied in size, intensity, and duration. Before, during, and after the storms, stream water samples were taken manually in five-to-seven-gallon aliquots. The stream sample just prior to the onset of precipitation was used to determine the old or pre-event water isotopic composition. To ensure a well-mixed sample, water was collected at different depths (from the surface to the bed) while sampling. This protocol was adopted to avoid biasing the suspended load composition by only collecting sediment at one sample depth. Additionally, just prior to and just after each storm, sediment from the streambed and margins was sampled from 10 sites throughout the upper watershed to determine a representative ^{7}Be activity for each of these sediment sources.

We sampled throughfall precipitation at the gage using a custom-built triangular collector that drained to five-gallon buckets. The 0.78 m^2 catching area of the collector captured enough volume for robust FRN analysis with every 0.25–0.5 cm of rainfall, allowing us to construct detailed intrastorm time series of rainfall and FRN fluxes to the watershed. We supplemented these time-resolved data with six storm-total throughfall precipitation samples, collected using five-gallon buckets dispersed throughout the watershed to capture variations with elevation and tree-canopy cover. In the field, we collected a 30 ml aliquot from each sample bucket for stable isotope analysis, filtering it to 0.45 μm (Fisher Scientific 25 mm nylon membrane). We then acidified the remainder of each sample to pH < 1 using trace-metal-grade HCl and transported all samples back to the lab to refrigerate for later analysis. The precipitation collector and five-gallon buckets were manually cleaned, soaked, and rinsed in water and dilute trace-metal-grade HCl between storm events to ensure no cross-storm contamination occurred. Although we recognize that the isotopic composition of precipitation varies throughout a storm (Pionke & Dewalle, 1992), for each event only the average composition of all throughfall samples was used in the mass balance.

As a point of comparison inspired by the analyses of the Middle Loup River data (Figure 2), for one large storm ($Q_{peak}/Q_2 = 0.8$) on 11 July 2021 we measured the suspended load concentration and flow depth along transects at increasing downstream distances along Mink Brook. We used these data to calculate the integrated suspended load mass as a function of distance from the channel edge. A least-squares best fit of Equations 6 and 9 to these data was then used to determine the fractional marginal area f and characteristic suspended load transport length L as a function of watershed area.

4.3. Precipitation and Stream Sample Filtration

Each stream water sample was progressively filtered using 20 μm ashless filter paper (Whatman 1441-090, 90 mm) and 0.5 μm glass fiber filters (Advantec GC-90, 90 mm) to collect suspended load. Precipitation samples generally had lower particulate concentrations and were filtered just with the 0.5 μm filters. Because ^{7}Be and ^{210}Pb may sorb to material finer than the smallest feasible filter cutoff or possibly even remain in ionic form, the method of Benitez-Nelson et al. (2001) was adapted as follows to induce flocculation of FRNs passing the 0.5 μm cutoff. To the 0.5 μm filtrate, sufficient concentrated HCl (37% w/w) was added to yield pH < 1 (~2% v/v HCl). After 24 hr equilibration, the sample pH was increased to ~9 with NH_4OH (28% w/w). Next, 60–120 μmol of $KMnO_4$ and 120 μmol of $MnCl_2$ were immediately added to the water to precipitate MnO_2. This sample was mixed and allowed to sit for at least 24 hr, to allow flocculation of MnO_2 that scavenged any remaining ^{7}Be and ^{210}Pb in the sample. The MnO_2 was subsequently filtered to 0.5 μm. The remaining filtrate was reacidified to pH < 1 for a final yield measurement. Total Be and Pb yields of the MnO_2 procedure were measured by spiking each acidified sample with ^{9}Be and stable Pb and measuring preprecipitation and postprecipitation aliquots by ICPOES. Yields were typically >90%.

After the isotopic analyses of the filtrate (see below), each suspended load filter was air-dried for 24 to 72 hr to remove residual water, then weighed to determine suspended load concentration. For carbon isotope analyses, 10–75 mg of dried sediment on the filter (depending on organic matter concentration) was encapsulated into tin (Sn) capsules and sent for ^{13}C isotopic analysis at the UC Davis Stable Isotope Facility. Organic matter content was then determined by loss-on-ignition (LOI) as the difference in sample mass before and after heating a representative sub-sample of the sediment for 4 hr at 550 °C.

4.4. Isotopic Analyses

The activities of ^{7}Be, ^{210}Pb, and ^{226}Ra (used to determine excess ^{210}Pb) were measured in situ using a high-purity germanium detector (Canberra model number BEGe3830) following the method described by Landis et al. (2012). The suspended load and MnO_2 filter samples were counted for 1–4 days in plastic 90 mm petri dishes placed directly on the HPGe detector endcap. Each bulk sediment sample taken from the margin or bed was sieved to 2 mm, packed and sealed into a 110 cm^3 plastic container, and counted for 4 days. Each sample count rate was corrected for decay, self-attenuation, detector efficiency, and interference from ^{228}Ac (Landis et al., 2012). To determine the amount of ^{7}Be in the stream due to precipitation, the stable hydrogen isotopic composition of the throughfall and each stream discharge sample was analyzed using a Picarro Water Vapor Isotope Analyzer (model L2130-i) using three reference standards.

5. Results

5.1. Storms

The 10 sampled storms varied in precipitation amount, intensity, and duration (Table 1). The median precipitation amount was 21 mm. The largest storm with 39.5 mm of precipitation occurred on 13 May 2017 and had a peak normalized discharge $Q/Q_2 = 0.36$. The smallest sampled storm with 8.2 mm of precipitation occurred on 20

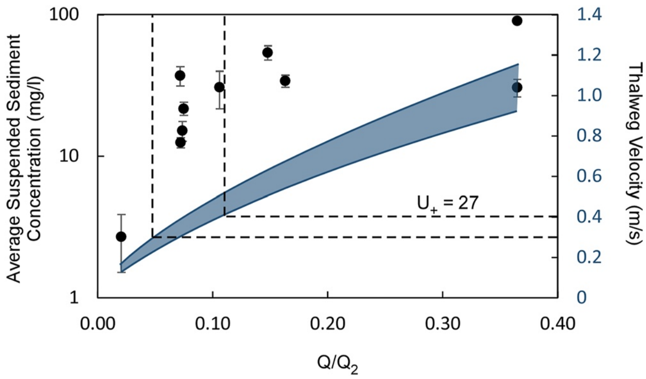

Figure 4. Storm average suspended load concentration (black symbols) and thalweg velocity (blue lines) versus normalized peak storm discharge. Range of estimated thalweg velocities corresponds to 1.2–1.5 times mean flow velocity at peak discharge. Dashed lines indicate flow velocities above which the effective settling velocity is near zero ($U_+ = 27$) for particle densities of 1.2 and 1.5 g/cm^3, respectively.

October 2017 and had a peak normalized discharge $Q/Q_2 = 0.02$. Average suspended load concentration increased rapidly with peak storm discharge until $Q/Q_2 \sim 0.1$, above which the average suspended load concentration was 48 ± 11 mg/L (Figure 4). This is consistent with an analysis USGS stream suspended load concentration measurements from 17 unregulated rivers in the Northeast U.S. region that found that the onset of significant suspended load concentrations occurs at a mean Q/Q_2 value of 0.06 ± 0.01 (Dethier et al., 2019). The thalweg velocity at $Q/Q_2 \sim 0.1$ approximately corresponds to the velocity at which the effective settling velocity is zero ($U_+ = 27$) for particle densities of 1.2–1.5 g/cm^3. We estimate the thalweg velocity as 1.2–1.5 times the mean flow velocity (Xia, 1997).

5.2. Stream and Throughfall Samples

For all storms, the measured suspended load concentrations were well correlated with turbidity, although the rating curves for summer storms (June to September) differed from that for spring and fall storms (Figure 5). The strong correlation with turbidity allows for a near continuous (every 15 min) record of suspended load concentrations that, coupled with discharge measurements, allows for the suspended load flux to be determined. The mean organic fraction based on the LOI measurements was 34 ± 19% (mean ± standard deviation) and generally decreased with increasing suspended load concentrations, ranging from ∼60% organic when the suspended load concentrations were low to ∼20% organic for the highest suspended load concentration samples.

Across all our storms, the ratio of throughfall to open fall ^{7}Be activity ranged from 9% to 77%, with a mean of 50 ± 21% (mean ± standard deviation). This is consistent with estimates of the fraction of ^{7}Be standing inventory found in vegetation canopy (Landis et al., 2014) and is similar to that observed by Karwan et al. (2018). For the Karwan data, excluding outliers where throughfall ^{7}Be was greater than open fall activity, the mean throughfall to open fall ^{7}Be activity ratio was 58 ± 17%. The effect of ^{7}Be scavenging in throughfall was neglected by Underwood et al. (2015). In order to compare our results to this earlier work, we reanalyzed the Underwood et al. (2015) data assuming that 50% of the precipitation ^{7}Be was scavenged in throughfall.

The average intrastorm variations in discharge (i.e., the average hydrograph), suspended load flux, ^{7}Be flux, and percent of export ^{7}Be in dissolved (<0.5 μm) phase are shown in in Figure S1 in Supporting Information S1. All the storms followed the same general temporal patterns in these parameters except the storm on 3 September 2017. While the hydrograph for this storm is similar to those of the other storms, the suspended load flux was much lower than observed in the other storms, likely reflecting a limited supply of suspended load in late summer.

5.3. Mass Balance

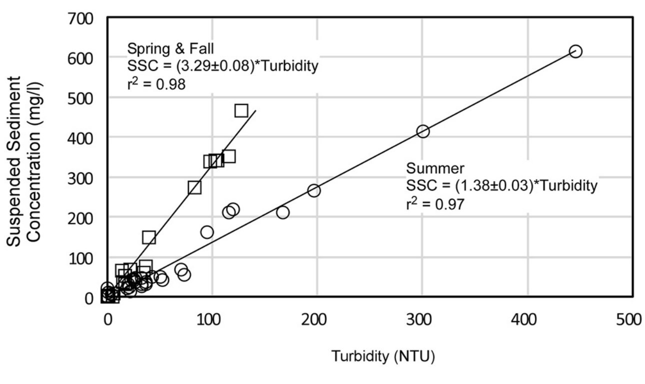

Figure 5. Suspended load rating curve relating turbidity to suspended load concentration.

Greater detail on the source and fate of suspended load is provided by the joint isotopic mass balance. A typical separation is shown in Figure 6. Consistent with previous observations (Le Gall et al., 2017; Salant et al., 2008; Underwood et al., 2015), the suspended load flux peaks near but before peak discharge, indicating a supply limited system typical of gravel-bedded streams. Accordingly, in calculating the storm average sediment fluxes, we use the time to peak discharge as the event duration. Prior to peak, the suspended load flux matches the rate of erosion of sediment from the bed; i.e., the suspended load is supplied from erosion of the bed rather than the channel margins. As discharge wanes after peak sediment flux, bed erosion continues at a reduced rate and begins to be offset by deposition on the channel margins, with ultimately erosion from the bed almost entirely offset by deposition on the margins later in the event. Integrated over the entire storm, 3,460 ± 266 kg of sediment were eroded from the bed upstream of the sampling location. Of that eroded mass, 40% (1,383 ± 216 kg) was deposited

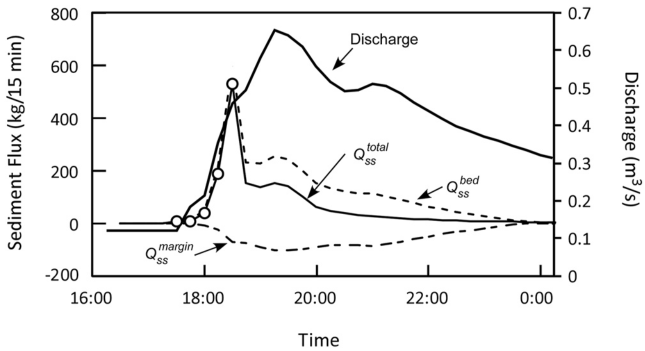

Figure 6. Variations in discharge and suspended load fluxes during the storm on 14 July 2016. Circles indicate times of discrete suspended load samples. Negative values for Q_{ss}^{margin} indicate deposition on channel margins while positive values for Q_{ss}^{bed} indicate erosion from the bed.

on the channel margins upstream of the sampling location and the remaining 60% (2,077 ± 50 kg) exported from the watershed. Using a representative bulk density of organic-rich margin sediment (1.2 g/cm^3), the mass deposited on the channel margins is equivalent to a depth of ∼0.023 ± 0.004 mm.

Consistent with the earlier work of Underwood et al. (2015), across all events the bed was a source and the channel margins a sink for suspended load. Not apparent in this earlier work, however, are the strong and consistent seasonal variations in margin deposition and fraction of suspended load exported out of the watershed (Figure 7). Comparing these parameters across the year, we find that, in general, the fraction of suspended load exported out of the watershed increases through the spring and summer (Figure 7b), resulting in less sediment deposited on the channel margins (Figure 7a). A plot of bed erosion over time would look similar to that shown for bed deposition in Figure 7a. That is, bed erosion also generally decreases though spring and summer. After leaf fall in later summer/early fall, bed erosion and deposition on the channel margins increase again and less of the suspended load is exported out of the watershed.

5.4. Sediment Exposure Age and Carbon Isotopic Composition

Few of the samples had detectable ^{226}Ra and hence we assumed that excess ^{210}Pb ≈ ^{210}Pb activity. The ratio of ^{7}Be to excess ^{210}Pb activities in suspended load is a factor of 4 lower than incident throughfall deposition and generally decreases over time (Figure 8), but on average is equivalent to an exposure age of 1–2 years (^{7}Be to excess ^{210}Pb activity ratio ∼2). This is consistent with the suspended load being at least partially composed of leaf fall from the previous year. Note that leaves falling into the stream in the fall have an exposure age of ∼half a year (^{7}Be to excess ^{210}Pb activity ratio ∼5) and thus, by the following spring and summer, have an exposure age of 1–2 years. Additional evidence for the aging of organic matter comes from the evolution of δ^{13}C in suspended load, with δ^{13}C also decreasing throughout the year (Figure 8). This likely reflects the preferential decomposition of high-quality carbon (e.g., lipids, amino acids, and some carbohydrates). Evolving δ^{13}C may also possibly indicate an increasing fraction of autochthonous carbon. For example, diatoms are common in the summer suspended load samples and Webb et al. (2016) observed that diatoms in UK rivers have a median δ^{13}C composition of −27.8 ± 1.0‰ (median ± standard deviation), similar to the isotopic compositions we observe in the late summer and fall.

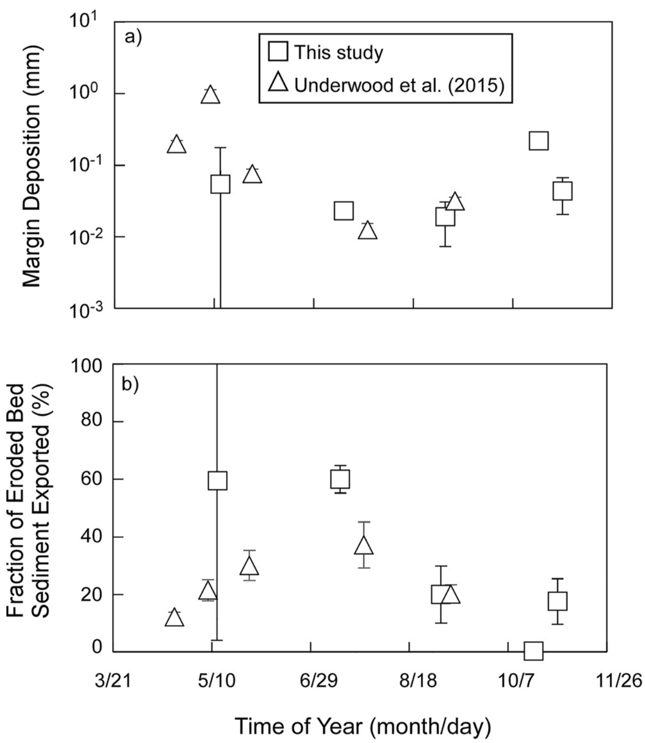

Figure 7. (a) Mass of sediment deposited on the channel margins upstream of the sampling location expressed as an equivalent depth. (b) Fraction of suspended load eroded from the channel bed upstream of the sampling location that is exported out of the watershed. The large uncertainty in the early May storm is due to the similarity of the bed and channel sediment ^{7}Be activity, resulting in poor separation of these end members in the mass balance (Equation 15).

5.5. Fractional Margin Size and Transport Length

The margin deposition rate per unit downstream distance Q_{ss}^{margin} predicted from hydraulic theory (Equation 10) is compared to the joint-isotopic rate (Equation 15) in Figure 9. We find a margin size fraction $f = 0.33$ results in reasonable agreement between the predicted (Equation 10) and observed (Equation 15) Q_{ss}^{margin} values. The largest misfit occurs for the smallest storm. Other than for the smallest storm, which has a small fractional margin size, the fractional margin size f is approximately uniform and apparently not strongly dependent on season or discharge.

The characteristic suspended load transport length L for each storm is shown in Figure 10. Here, the average channel flow velocity is set equal to the storm average flow velocity at the sampling site and is assumed not to vary significantly over the transport length. Surprisingly, except for the smallest storm where the flow velocity was not sufficient to fully suspend the sediment

10.1029/2021WR031212

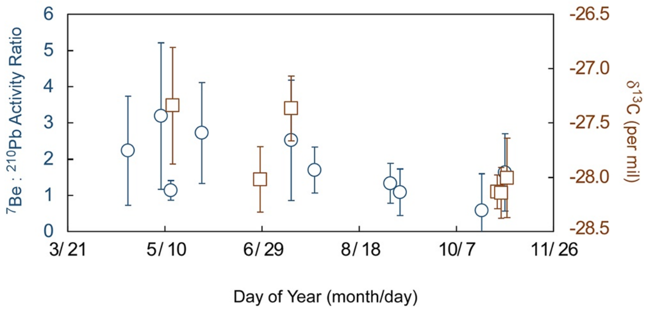

Figure 8. Annual variation in ^{7}Be to excess ^{210}Pb activity ratio (blue circles) and carbon isotopic composition (brown squares) of suspended load. Carbon isotopic composition is in ‰ relative to the standard Vienna Pee Dee Belemnite. Errors bars are ± one standard deviation.

(Figure 4), the transport length is more or less independent of storm size (and season), with an average value of 5.8 km ± 1.6 km (mean ± standard error).

5.6. Channel Transects of Integrated Sediment Mass

Finally, the variation in integrated sediment mass as a function of distance from the channel edge for the large storm ($Q_{peak}/Q_2 = 0.8$) is shown in Figure 11 along with the least-squares best fit of Equations 6 and 9. Although the data are scattered, the data from all the transects follow the model trend. The mean of the best fit fractional areas f across all transects was 0.23 ± 0.05 (mean ± standard deviation), similar, albeit slightly less than, the typical value at the former USGS gage determined using isotopic mass balance (Figure 11).

6. Discussion

6.1. Source of Suspended Load

Bilby and Likens (1980) showed that organic debris dams are important in accumulating and temporarily storing coarse particulate organic matter in channels, with debris dams containing nearly 75% of the standing stock of organic matter in first order streams. In recently glaciated regions such as northern New England, sediment production and fluxes are generally anomalously low (Kaste et al., 2007; Rainwater, 1962). Low-order channels are often partly confined and hence have low rates of bank retreat (Pizzuto et al., 2018). Thus, in these regions, the annual influx of organic debris is a significant fraction of the suspended load budget, especially during moderate storm events where the suspension of inorganic particles is suppressed by their higher densities. This inference is consistent with previous studies showing that in headwater channels, and particularly in cooler climates which tend to limit autochthonous net primary productivity, terrestrial allochthonous detrital material is a primary source of particulate organic matter (Allan & Castillo, 2007; Sutfin et al., 2016; Vannote et al., 1980). The apparent exposure age of the particles of 1–2 years is consistent with the idea that the FRNs are tracing suspended load from the annual influx of organic debris after leaf fall.

Allochthonous detrital material serves as a key food resource for both shredding and nonshredding macroinvertebrates and thus is broken down into finer particles by invertebrates and microbes within the channel, on the floodplain, and within the subsurface (Richardson, 1992; Sutfin et al., 2016; Wagener et al., 1998). The systematically decreasing bulk δ^{13}C of suspended load throughout the summer and fall reflects the preferential decomposition of high-quality carbon (e.g., lipids, amino acids, and some carbohydrates). This preferential decomposition changes the character of the suspended load (Richardson et al., 2009), as evidenced by the changing correlation between suspended load concentrations and turbidity (Figure 5). That the supply of suspended load is limited by its rate of decomposition is also consistent with the hysteresis of the suspended load concentration versus discharge relationship (Le Gall et al., 2017; Salant et al., 2008; Underwood et al., 2015).

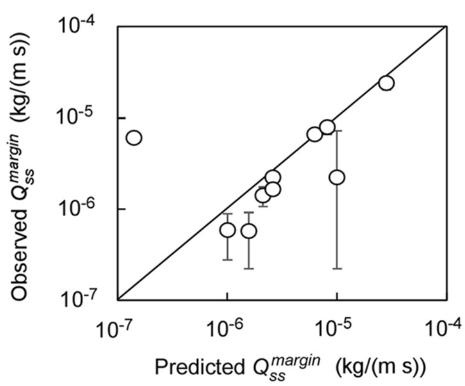

Figure 9. Predicted (Equation 10) versus observed (Equation 15) Q_{ss}^{margin} with the lateral margin size fraction $f = 0.33$.

At a similarly sized watershed in southeastern Pennsylvania (USA) having more agriculture and development, Rose et al. (2018) argued that during low to moderate discharge events, a significant fraction of suspended load is derived from in-stream processes including redox-controlled precipitation reactions and subsequent adsorption between organic matter and metal-oxides. That some of the suspended particles at their site were newly created is consistent with the young exposure ages of a few months or less of some of the suspended particles inferred from their radionuclide activity ratios (Karwan et al., 2018). While redox-controlled precipitation undoubtedly occurs at in Mink Brook groundwater mixes with more oxic stream water, the underlying geology at Mink Brook is less conducive to redox precipitation. In the Pennsylvania watershed, carbonate-rich bedrock in the headwaters contributes well-oxygenated, higher pH stream water that then mixes

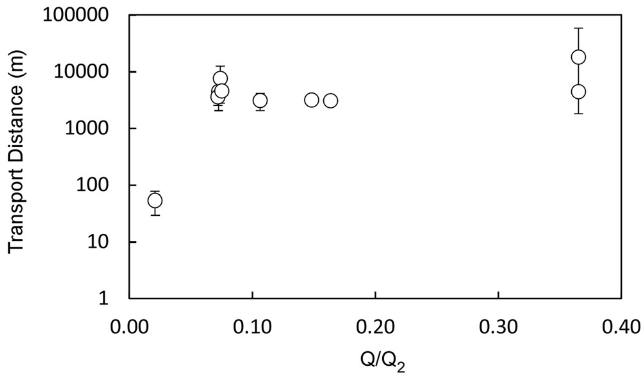

Figure 10. Characteristic suspended load transport length L for each storm.

downstream with less oxic, lower pH water draining riparian wetlands and buried wetland layers (Rose et al., 2018; Walter & Merritts, 2008). The Mink Brook watershed is entirely underlain by crystalline metamorphic rocks mantled by ~1–2 m deposits of glacial sediments with limited riparian wetlands. Thus, most of the groundwater entering the stream is derived from relatively shallow flow paths that are more oxygenated than deeper groundwater flow pathways. The radionuclide activity ratios of the suspended load in Mink Brook are all consistent with exposure ages of greater than 1 year and thus not consistent with newly precipitated particles seen by Karwan et al. (2018).

6.2. Seasonal Variation in Sediment Trapping

The limited supply of the evolving suspended load results in seasonal variations in the fraction of suspended load that is exported out of the watershed. Especially during the spring and fall when suspended load fluxes are greatest, only a small fraction (<~20%) of the suspended load is exported from the watershed (Figure 7b). Most of the suspended load is deposited on the channel margins (Figure 7a). Even in the summer, when the export of suspended load may be facilitated by the more highly decomposed nature of the sediment, nearly half of the suspended load is trapped by the channel margins. Thus, while in-stream organic carbon storage is limited, the channel still serves an important role in the decomposition of organic carbon and as a source of organic carbon to the channel margins (Hall et al., 2009; Pinay et al., 1992; Tank et al., 2010). In an analysis of particulate nitrogen residence times in a mountain stream, Hall et al. (2009) similarly concluded that the stream is not an effective conduit for particulate nutrients.

The characteristics of Mink Brook facilitate the trapping of suspended load, including channel complexity that results in slower flow velocities that favor deposition and foster hotspots for organic matter decomposition (Battin et al., 2008; Dunne & Leopold, 1978; Sutfin et al., 2016). Systems with less channel complexity and/or larger systems may flush suspended load more efficiently. For example, in Mink Brook, we find that the depositional margins occupy as much as two-thirds of the channel, whereas in Figure 2, we find that the channel margins only occupy about one-third of the larger Middle Loup River (Hubbell & Matejka, 1959).

6.3. Watershed Size Effects

Vannote et al. (1980) proposed that organic matter transport, storage, and use by macroinvertebrates are regulated by fluvial geomorphic processes such that biological communities are in equilibrium with the dynamic physical conditions of the channel. In Mink Brook, this is manifested by a balance between allochthonous organic matter inputs, primarily in the fall, and the rate at which organic matter is decomposed and deposited onto the channels margins over the rest of the year. The late summer shift to suspended load with older exposure ages (Figure 8) and peaks in suspended load flux well before peak discharge (Figure S1b in Supporting Information S1) indicate that the abundant source of suspended load in the fall and spring is exhausted by late summer. Under the river continuum concept (Doretto et al., 2020; Vannote et al., 1980), as stream size increases, the importance of terrestrial organic input decreases as autochthonous primary production and organic transport from upstream increases. Thus, in the headwaters of Mink Brook above our sampling site, we expect the allochthonous supply of organic matter to the channel exceeds the rate at which it is decomposed, resulting in a large net flux of organic matter to the channel margins and floodplains. Conversely, at some distance downstream of our sampling site, the rate of decomposition of the allochthonous supply of organic matter is sufficient to exhaust the supply and autochthonous primary production is the dominant source of organic matter for at least part of the year (Vannote et al., 1980). The decreasing role of channel margins in

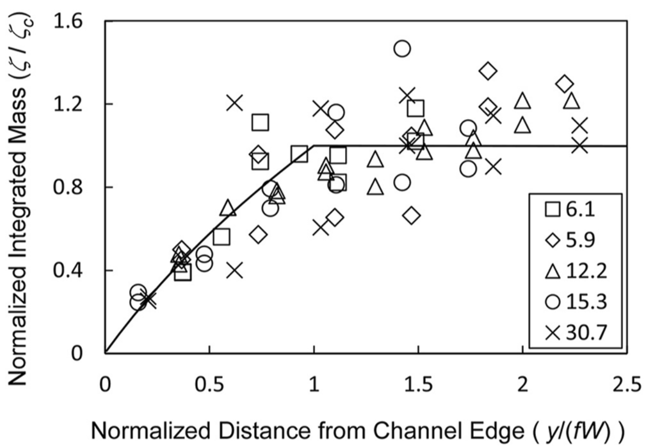

Figure 11. Integrated sediment masses as a function of distance from the channel edge along transects at increasing downstream distances along Mink Brook. Legend indicated watershed area (km^2) at which each transect was measured. Solid line is variation predicted by Equations 6 and 9.

10.1029/2021WR031212

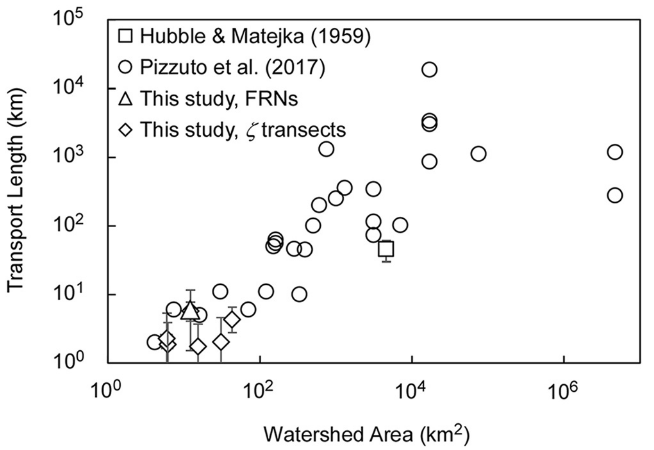

Figure 12. Suspended load characteristic transport length data with predicted scaling (solid line). Note that Pizzuto et al. (2017) summarized length scale data from a variety of studies and authors. The Hubbel and Matejka (1959) length scale is from section C, Middle Loup River. Triangles are data from Figure 10, diamonds are data from Figure 11.

trapping suspended load with increasing watershed size is consistent with the smaller margin fraction ($f = 0.18$) of the larger Middle Loup River (watershed area = 4,600 km^2; Hubbell & Matejka, 1959) compared to Mink Brook ($f = 0.33$, watershed area = 12 km^2).

The decreasing role of channel margins in trapping suspended load with increasing watershed size is also consistent with the larger characteristic suspended load transport length of the Middle Loup River compared to Mink Brook. Using Equation 13 with the best fit values from Equation 10 (Figure 2b), we estimate L = 100 km for the Middle Loup River (Hubbell & Matejka, 1959), versus L = 5.8 km ± 1.6 km for Mink Brook from the FRN data. Characteristic transport lengths from the transect data (Figure 11) increase slightly with increasing watershed area. However, we emphasize that while the transport length at the former gage site is well constrained by multiple measurements across different seasons (Figure 12), the transport lengths from the transect data are only from a single storm and thus less well constrained. While the data indicate increasing transport length with increasing watershed area, the data are not sufficiently robust to warrant speculation regarding the form of that increase.

Adapting the nutrient spiraling analysis of Newbold et al. (1981) and Cushing et al. (1993), Whiting et al. (2005) estimated the characteristic suspended load transport length based on the downstream exponential decay of sediment tracer concentrations. They also estimated the increase in transport length with increasing drainage basin area assuming the advected travel distance scales with the average flow velocity and the particle settling time. However, Whiting et al. (2005) note that the Rouse number for sampled sediment during transport is sufficiently large that the sediment is expected to remain suspended rather than settle. Pizzuto et al. (2017) summarized the results of Whiting et al. (2005) along with estimates of the transport length based on sediment budgets reported in the literature. Figure 12 compares their data to the transport length scales reported here. As noted by Pizzuto et al. (2017), the systematic scaling of transport length with watershed area deteriorates for watershed areas $A > 10^4$ km^2, but for smaller watersheds the Mink Brook transport lengths are in reasonable agreement with the previously reported values and with the increasing transport length with watershed area.

Vannote et al. (1980) proposed that the gradient in physical conditions along a river results in a continuum of biotic adjustments with respect to the transport and storage of organic matter. Terrestrial allochthonous detrital material entering headwater streams is the primary source of organic matter input to river systems (Battin et al., 2008; Gomi et al., 2002; Kaushik & Hynes, 1971; Sutfin et al., 2016). As watershed size increases, the relative proportion of terrestrial inputs of organic matter decreases as rivers widen and receive more abundant sunlight and autochthonous primary production becomes a more significant source (Cummins, 1975; Galy et al., 2015; Sutfin et al., 2016). In this manner, terrestrial inputs are systematically decoupled from the channel with increasing watershed area (Gomi et al., 2002). In addition, decreasing terrestrial inputs are coupled with declining in-stream storage volumes and storage times with increasing discharge (Battin et al., 2008). The results from this study showing increased transport length with increasing watershed area provide a physical mechanism for this decoupling. Decreasing terrestrial inputs result in a lower rate of increase in Q_{ss}^{margin} with watershed area compared to the rate of increase in the mixing volume (WH), increasing the mixing time (Equation 12) and transport length (Equation 13). The increase in transport length implies that as watershed area increases, suspended particles travel further before settling on the channel margins. The decreased rate of particle delivery to the margins with increasing watershed area is reflected in decreasing relative margin size (f) and the decline in in-stream storage.

6.4. Caveats

There are some important caveats and limitations to the above analysis. First, as noted by Bradley and Tucker (2013), sediment particles in fluvial systems spend the majority of their total transit time at rest. Radiocarbon dating of channel margin deposits in the South River (VA, USA) indicate ages from 1 to >60 years with an average turnover time of 1.75 years (Skalak & Pizzuto, 2010), similar to the exposure age of the suspended load we sampled. Although beyond the scope of the present work, a complete analysis of the sediment budget

10.1029/2021WR031212

requires quantification of particle rest times, as recently done by Pizzuto (2020). Second, significant sediment transport only occurs during flows sufficient to suspend sediment, which for Mink Brook occurs for $Q/Q_2 > \sim 0.1$ (Figures 4 and 10). The corresponding upper bound discharge for the transport we observe is less clear but certainly less than bankfull and may be a function of sediment availability and hence land use. For discharge events less than bankfull, the apparent sediment exposure age and $\delta^{13}C$ composition indicate that the FRNs primarily trace the source and fate of organic-rich suspended load. During the Hurricane Irene extreme precipitation event over White Clay Creek (PA, USA), Rose et al. (2018) observed that suspended particulate matter collected shortly after peak discharge was derived from near-stream sources (i.e., streambed and floodplain deposits), whereas suspended particulate matter collected later in the event was more similar to extra-channel sources (i.e., zero-order gullies). In addition, higher discharge events will mobilize higher density inorganic particles. For example, we observed that the organic fraction of suspended load based on the LOI measurements decreased with increasing suspended load concentrations. Kaste et al. (2014) showed that even unweathered coarse-grained sediments retain ^{7}Be and thus FRNs are still viable tracer of sediment flux even in the absence of organic matter; however, the potential area for sediment deposition and storage expands as the floodplains are inundated (Pizzuto, 1987). Numerous studies have highlighted the role of floodplains as important sinks or stores for suspended load, trapping between about one-quarter to one-half of the total suspended load transported (see Walling et al., 1996). This is a smaller fraction of the total suspended load than we observed trapped by channel margins in our moderate discharge events (Figure 7b), yet still highlights the important role of sediment trapping in the overall suspended load budget.

7. Conclusions

We find that across all moderate discharge events (recurrence intervals from a few weeks to a few months), the channel bed was a source of organic-rich (LOI of 20–60%) suspended load and the channel margins a sink. This observation is consistent with the earlier work of Underwood et al. (2015). Novel in this work is the observation of strong and consistent seasonal variation in the fraction of suspended load exported out of the watershed. In general, the fraction of suspended load exported out of the watershed increases through the spring and summer, resulting in less sediment deposited on the channel margins. After leaf fall in late summer/early fall, bed erosion and deposition on the channel margins increase again and only a small fraction (<20%) of the suspended load is exported out of the watershed. The exposure age of the suspended load is consistent with that of the prior year's litterfall. The increased fraction of suspended load exported out of the watershed in the summer may be partly a result of the changing character of the suspended load, as indicated by its changing bulk $\delta^{13}C$ composition and changing relationship between turbidity and suspended load concentration. These changes likely reflect the decomposition of the organic matter within the channel and possibly a small but increasing contribution of autochthonous carbon (e.g., diatoms). That the available organic matter is limited by its rate of decomposition is consistent with the hysteresis of the suspended load concentration versus discharge relationship. Thus, while in-stream organic carbon storage is limited, the channel still serves an important role in the decomposition of organic carbon and as a source of organic carbon to the channel margins.

The characteristics of headwater streams facilitate the trapping of suspended load that limit its export, including significant channel complexity that results in slower flow velocities that favor deposition and foster hotspots for organic matter decomposition (Battin et al., 2008; Dunne & Leopold, 1978; Sutfin et al., 2016). The apparent exposure age of the suspended load in Mink Brook is similar to the average turnover time of channel margin deposits reported by Skalak and Pizzuto (2010). The trapping of suspended load in the channel margins limits the characteristic transport distance of suspended load, which we find, given sufficient discharge to fully suspend the sediment, is nearly independent of stream discharge (and season) for sub-bankfull discharges. Decreasing fractional margin size with increasing watershed area results in a corresponding increase in transport length consistent with previous observations and indicates a systematic decoupling of the channel from terrestrial organic matter inputs.

The results presented here provide a framework for understanding suspended load dynamics in glaciated regions such as northern New England where sediment production and fluxes are generally low and thus the annual input of organic debris a major component of suspended load budget. However, additional work is needed to fully understand the implications of these dynamics. For example, vegetation is known to efficiently trap atmospheric Hg emissions (Jiskra et al., 2018) and litterfall dominates the Hg flux to forested ecosystems (Bishop et al., 2020). Where particulate organic carbon concentrations are high, particulate Hg is the major form of Hg leaving the catchment in runoff (Shanley et al., 2008). Yet it remains unclear how the in-channel decomposition of organic debris affects the fate and transport of particulate Hg and, in particular, the partitioning between exported particulate Hg and particulate Hg deposited on the channel margins. Hsu-Kim et al. (2018) argue that the development of models that capture the complexity of fluvial Hg concentrations and fluxes remains a major unmet research need. Similarly, Boyero et al. (2011) found that climate warming will likely hasten microbial litter decomposition while decreasing detritivore-mediated decomposition rates, resulting in no overall change in organic matter decomposition rates. Nevertheless, the shift in importance from detritivores to microbes in warmer climates would likely increase CO_2 production and decrease the generation of recalcitrant organic particles. It remains unclear how this possible shift in decomposition rates would impact the export of carbon-rich suspended load, which exerts an important control on watershed-scale carbon fluxes.

Data Availability Statement

All data from this work are available at www.hydroshare.org/resource/3fcc058d3bf24d49a470f97c73c5d79e.

Acknowledgments
We thank the three anonymous reviewers for the helpful suggestions. We also thank N. Renshaw for her help in the field. This work was supported by funding from the National Science Foundation (EAR-1545623).

References

Allan, J. D., & Castillo, M. M. (2007). *Stream ecology*. New York, NY: Springer.

Aufdenkampe, A. K., Mayorga, E., Raymond, P. A., Melack, J. M., Doney, S. C., Alin, S. R., et al. (2011). Riverine coupling of biogeochemical cycles between land, oceans, and atmosphere. *Frontiers in Ecology and the Environment*, *9*(1), 53–60. https://doi.org/10.1890/100014

Battin, T. J., Kaplan, L. A., Findlay, S., Hopkinson, C. S., Marti, E., Packman, A. I., et al. (2008). Biophysical controls on organic carbon fluxes in fluvial networks. *Nature Geoscience*, *1*(2), 95–100. https://doi.org/10.1038/ngeo101

Benda, L., & Dunne, T. (1997). Stochastic forcing of sediment supply to channel networks from landsliding and debris flow. *Water Resources Research*, *33*(12), 2849–2863. https://doi.org/10.1029/97WR02388

Benitez-Nelson, C. R., Buesseler, K. O., van der Loeff, M. R., Andrews, J., Ball, L., Crossin, G., & Charette, M. A. (2001). Testing a new small-volume technique for determining Th-234 in seawater. *Journal of Radioanalytical and Nuclear Chemistry*, *248*(3), 795–799. https://doi.org/10.1023/a:1010621618652

Bilby, R. E., & Likens, G. E. (1980). Importance of organic debris dams in the structure and function of stream ecosystems. *Ecology*, *61*(5), 1107–1113. https://doi.org/10.2307/1936830

Bishop, K., Shanley, J. B., Riscassi, A., de Wit, H. A., Eklöf, K., Meng, B., et al. (2020). Recent advances in understanding and measurement of mercury in the environment: Terrestrial Hg cycling. *Science of the Total Environment*, *721*, 137647. https://doi.org/10.1016/j.scitotenv.2020.137647

Bonniwell, E. C., Matisoff, G., & Whiting, P. J. (1999). Determining the times and distances of particle transit in a mountain stream using fallout radionuclides. *Geomorphology*, *27*(1–2), 75–92. https://doi.org/10.1016/s0169-555x(98)00091-9

Boyero, L., Pearson, R. G., Gessner, M. O., Barmuta, L. A., Ferreira, V., Graça, M. A. S., et al. (2011). A global experiment suggests climate warming will not accelerate litter decomposition in streams but might reduce carbon sequestration. *Ecology Letters*, *14*(3), 289–294. https://doi.org/10.1111/j.1461-0248.2010.01578.x

Bradley, D. N., & Tucker, G. E. (2013). The storage time, age, and erosion hazard of laterally accreted sediment on the floodplain of a simulated meandering river. *Journal of Geophysical Research: Earth Surface*, *118*, 1308–1319. https://doi.org/10.1002/jgrf.20083

Brummer, C. J., & Montgomery, D. R. (2003). Downstream coarsening in headwater channels. *Water Resources Research*, *39*(10), 1294. https://doi.org/10.1029/2003WR001981

Carter, J., Walling, D. E., Owens, P. N., & Leeks, G. J. L. (2006). Spatial and temporal variability in the concentration and speciation of metals in suspended sediment transported by the River Aire, Yorkshire, UK. *Hydrological Processes*, *20*(14), 3007–3027. https://doi.org/10.1002/hyp.6156

Chartin, C., Evard, O., Onda, Y., Patin, J., Lefevre, I., Ottle, C., et al. (2013). Tracking the early dispersion of contaminated sediment along rivers draining the Fukushima radioactive pollution plume. *Anthropocene*, *1*, 23–34. https://doi.org/10.1016/j.ancene.2013.07.001

Clark, C. J. (2017). *Determining maximum suspended-particle size in a channel flow* (p. 29). Hanover, NH: Dartmouth.

Cummins, K. W. (1975). The ecology of running waters: Theory and practice. In D. B.Baker, W. B.Jackson, & B. L.Prater (Eds.), *Proceedings of the Sandusky River Basin Symposium* (pp. 277–293). Oak Ridge, TN: Energy Research and Development Administration.

Cushing, C. E., Minshall, G. W., & Newbold, J. D. (1993). Transport dynamics of fine particulate organic-matter in 2 Idaho streams. *Limnology & Oceanography*, *38*(6), 1101–1115. https://doi.org/10.4319/lo.1993.38.6.1101

Dethier, E. N., Renshaw, C. E., & Magilligan, F. J. (2019). Temporal and spatial variations in watershed connectivity dictate suspended sediment source and fate. In *Annual Meeting of the American Geophysical Union* (pp. EP51C-2103), San Francisco.

Doretto, A., Piano, E., & Larson, C. E. (2020). The river continuum concept: Lessons from the past and perspectives for the future. *Canadian Journal of Fisheries and Aquatic Sciences*, *77*(11), 1853–1864. https://doi.org/10.1139/cjfas-2020-0039

Droppo, I. G. (2001). Rethinking what constitutes suspended sediment. *Hydrological Processes*, *15*(9), 1551–1564. https://doi.org/10.1002/hyp.228

Dunne, T., & Leopold, L. B. (1978). *Water and environmental planning*. New York, NY: W. H. Freeman.

Engelund, F. (1970). Instability of erodible beds. *Journal of Fluid Mechanics*, *42*, 225. https://doi.org/10.1017/s0022112070001210

Feng, X. H. (2002). A theoretical analysis of carbon isotope evolution of decomposing plant litters and soil organic matter. *Global Biogeochemical Cycles*, *16*(4), 1119. https://doi.org/10.1029/2002GB001867

Fisher, S. G., & Likens, G. E. (1972). Stream ecosystem: Organic energy budget. *BioScience*, *22*, 33–35. https://doi.org/10.2307/1296183

Fisher, S. G., & Likens, G. E. (1973). Energy flow in Bear Brook, New Hampshire—Integrative approach to stream ecosystem metabolism. *Ecological Monographs*, *43*(4), 421–439. https://doi.org/10.2307/1942301

Fryirs, K. (2013). (Dis)Connectivity in catchment sediment cascades: A fresh look at the sediment delivery problem. *Earth Surface Processes and Landforms*, *38*(1), 30–46. https://doi.org/10.1002/esp.3242

Galy, V., Peucker-Ehrenbrink, B., & Eglinton, T. (2015). Global carbon export from the terrestrial biosphere controlled by erosion. *Nature*, *521*(7551), 204–207. https://doi.org/10.1038/nature14400

Garcia, M. H. (2007). Sediment transport and morphodynamics. In *Sedimentation engineering: Processes, measurements, modeling, and practice* (pp. 21–163). Reston, VA: American Society of Engineers.

Gellis, A. C., Fuller, C. C., & Van Metre, P. C. (2017). Sources and ages of fine-grained sediment to streams using fallout radionuclides in the Midwestern United States. *Journal of Environmental Management*, *194*, 73–85. https://doi.org/10.1016/j.jenvman.2016.06.018

Genereux, D. P., & Hooper, R. P. (1998). Oxygen and hydrogen isotopes in rainfall-runoff studies. In C.Kendall, & J. J.McDonnell (Eds.), *Isotope tracers in catchment hydrology* (pp. 319–346). New York, NY: Elsevier. https://doi.org/10.1016/b978-0-444-81546-0.50017-3

Gibbs, R. J. (1973). Mechanisms of trace metal transport in rivers. *Science*, *180*(4081), 71–73. https://doi.org/10.1126/science.180.4081.71

Gomi, T., Sidle, R. C., & Richardson, J. S. (2002). Understanding processes and downstream linkages of headwater systems. *BioScience*, *52*(10), 905–916. https://doi.org/10.1641/0006-3568(2002)052[0905:Upadlo]2.0.Co;2

Hall, R. O., Baker, M. A., Arp, C. D., & Koch, B. J. (2009). Hydrologic control of nitrogen removal, storage, and export in a mountain stream. *Limnology & Oceanography*, *54*(6), 2128–2142. https://doi.org/10.4319/lo.2009.54.6.2128

Hamm, N. T., Dade, W. B., & Renshaw, C. E. (2009). Fine particle deposition to initially starved, stationary, planar beds. *Sedimentology*, *56*(7), 1976–1991. https://doi.org/10.1111/j.1365-3091.2009.01065.x

Hamm, N. T., Dade, W. B., & Renshaw, C. E. (2011). Fine particle deposition to porous beds. *Water Resources Research*, *47*, W11508. https://doi.org/10.1029/2010WR010295

Hornbeck, J. W. (1973). Storm flow from hardwood-forested and cleared watersheds in New Hampshire. *Water Resources Research*, *9*(2), 346–354. https://doi.org/10.1029/WR009i002p00346

Horowitz, A. J. (1995). *The use of suspended sediment and associated trace elements in water quality studies* (Vol. 4, pp. 18–52). IAHS Special Publication.

Hsu-Kim, H., Eckley, C. S., Acha, D., Feng, X. B., Gilmour, C. C., Jonsson, S., & Mitchell, C. P. J. (2018). Challenges and opportunities for managing aquatic mercury pollution in altered landscapes. *Ambio*, *47*(2), 141–169. https://doi.org/10.1007/s13280-017-1006-7

Hubbell, D. W., & Matejka, D. Q. (1959). Investigations of sediment transportation Middle Loup River at Dunning, Nebraska. *U.S. Geological Survey Water Supply Paper*, *1476*, 1–123.

Jiskra, M., Sonke, J. E., Obrist, D., Bieser, J., Ebinghaus, R., Myhre, C. L., et al. (2018). A vegetation control on seasonal variations in global atmospheric mercury concentrations. *Nature Geoscience*, *11*(4), 244–250. https://doi.org/10.1038/s41561-018-0078-8

Karwan, D. L., Pizzuto, J. E., Aalto, R., Marquard, J., Harpold, A., Skalak, K., et al. (2018). Direct channel precipitation and storm characteristics influence short-term fallout radionuclide assessment of sediment source. *Water Resources Research*, *54*, 4579–4594. https://doi.org/10.1029/2017WR021684

Kaste, J. M., Heimsath, A. M., & Bostick, B. C. (2007). Short-term soil mixing quantified with fallout radionuclides. *Geology*, *35*(3), 243–246. https://doi.org/10.1130/g23355a.1

Kaste, J. M., Magilligan, F. J., Renshaw, C. E., Fisher, G. B., & Dade, W. B. (2014). Seasonal controls on meteoric 7Be in coarse-grained river channels. *Hydrological Processes*, *28*(5), 2738–2748. https://doi.org/10.1002/hyp.9800

Kaushik, N. K., & Hynes, H. B. N. (1971). Fate of dead leaves that fall into streams. *Archiv fur Hydrobiologie*, *68*(4), 465.

Kendall, C., & Caldwell, E. A. (1998). Fundamentals of isotope geochemistry. In C.Kendall, & J. J.McDonnell (Eds.), *Isotope tracers in catchment hydrology* (pp. 51–86). New York, NY: Elsevier. https://doi.org/10.1016/b978-0-444-81546-0.50009-4

Landis, J. D., Hamm, N. T., Renshaw, C. E., Dade, W. B., Magilligan, F. J., & Gartner, J. D. (2012). Surficial redistribution of fallout (131)iodine in a small temperate catchment. *Proceedings of the National Academy of Sciences of the United States of America*, *109*(11), 4064–4069. https://doi.org/10.1073/pnas.1118665109

Landis, J. D., Renshaw, C. E., & Kaste, J. M. (2012). Measurement of Be-7 in soils and sediments by gamma spectroscopy. *Chemical Geology*, *291*, 175–185. https://doi.org/10.1016/j.chemgeo.2011.10.007

Landis, J. D., Renshaw, C. E., & Kaste, J. M. (2014). Quantitative retention of atmospherically deposited elements by native vegetation is traced by the fallout radionuclides Be-7 and Pb-210. *Environmental Science & Technology*, *48*(20), 12022–12030. https://doi.org/10.1021/es503351u

Le Gall, M., Evrard, O., Foucher, A., Laceby, J. P., Salvador-Blanes, S., Maniere, L., et al. (2017). Investigating the temporal dynamics of suspended sediment during flood events with Be-7 and Pb-210(xs) measurements in a drained lowland catchment. *Scientific Reports*, *7*, 42099. https://doi.org/10.1038/srep42099

Lyons, J. B., Bothner, W. A., Moench, R. H., & Thompson, J. B. (1997). *Bedrock geologic map of New Hampshire*. Reston, VA: U.S. Geological Survey.

MacDonald, L. H., & Coe, D. (2007). Influence of headwater streams on downstream reaches in forested areas. *Forest Science*, *53*(2), 148–168.

Newbold, J. D., Elwood, J. W., Oneill, R. V., & Vanwinkle, W. (1981). Measuring nutrient spiralling in streams. *Canadian Journal of Fisheries and Aquatic Sciences*, *38*(7), 860–863. https://doi.org/10.1139/f81-114

Nino, Y., Lopez, F., & Garcia, M. (2003). Threshold for particle entrainment into suspension. *Sedimentology*, *50*(2), 247–263. https://doi.org/10.1046/j.1365-3091.2003.00551.x

Parker, G. (1978). Self-formed straight rivers with equilibrium banks and mobile bed. 1. Sand-silt river. *Journal of Fluid Mechanics*, *89*(1), 109–125. https://doi.org/10.1017/s0022112078002499

Pinay, G., Fabre, A., Vervier, P., & Gazelle, F. (1992). Control of C, N, P distribution in soils of riparian forests. *Landscape Ecology*, *6*(3), 121–132. https://doi.org/10.1007/bf00130025

Pionke, H. B., & Dewalle, D. R. (1992). Intrastorm and interstorm O-18 trends for selected rainstorms in Pennsylvania. *Journal of Hydrology*, *138*(1–2), 131–143. https://doi.org/10.1016/0022-1694(92)90160-w

Pizzuto, J. (2020). Suspended sediment and contaminant routing with alluvial storage: New theory and applications. *Geomorphology*, *352*, 106983. https://doi.org/10.1016/j.geomorph.2019.106983

Pizzuto, J., Keeler, J., Skalak, K., & Karwan, D. (2017). Storage filters upland suspended sediment signals delivered from watersheds. *Geology*, *45*(2), 151–154. https://doi.org/10.1130/g38170.1

Pizzuto, J., O'Neal, M. A., Narinesingh, P., Skalak, K., Jurk, D., Collins, S., & Calder, J. (2018). Contemporary fluvial geomorphology and suspended sediment budget of the partly confined, mixed bedrock-alluvial South River, Virginia, USA. *Geological Society of America Bulletin*, *130*(11–12), 1859–1874. https://doi.org/10.1130/b31759.1

Pizzuto, J., Schenk, E. R., Hupp, C. R., Gellis, A., Noe, G., Williamson, E., et al. (2014). Characteristic length scales and time-averaged transport velocities of suspended sediment in the mid-Atlantic Region, USA. *Water Resources Research*, *50*, 790–805. https://doi.org/10.1002/2013WR014485

Pizzuto, J. E. (1987). Sediment diffusion during overbank flows. *Sedimentology*, *34*, 301–317. https://doi.org/10.1111/j.1365-3091.1987.tb00779.x

Porto, P., Walling, D. E., & Callegari, G. (2013). Using ^{137}Cs and ^{210}Pbex measurements to investigate the sediment budget of a small forested catchment in southern Italy. *Hydrological Processes*, *27*(6), 795–806. https://doi.org/10.1002/hyp.9471

Rainwater, F. H. (1962). *Stream composition of the Coterminous United States*. Washington, DC: U.S. Geological Survey.

Renshaw, C. E., Abengoza, K., Magilligan, F. J., Dade, W. B., & Landis, J. D. (2014). Impact of flow regulation on near-channel floodplain sedimentation. *Geomorphology*, *205*, 120–127. https://doi.org/10.1016/j.geomorph.2013.03.009

Renshaw, C. E., Feng, X. H., Sinclair, K. J., & Dums, R. H. (2003). The use of stream flow routing for direct channel precipitation with isotopically-based hydrograph separations: The role of new water in stormflow generation. *Journal of Hydrology*, *273*(1–4), 205–216. https://doi.org/10.1016/s0022-1694(02)00392-x

Richardson, D. C., Kaplan, L. A., Newbold, J. D., & Aufdenkampe, A. K. (2009). Temporal dynamics of seston: A recurring nighttime peak and seasonal shifts in composition in a stream ecosystem. *Limnology & Oceanography*, *54*(1), 344–354. https://doi.org/10.4319/lo.2009.54.1.0344

Richardson, J. S. (1992). Food, microhabitat, or both—Macroinvertebrate use of leaf accumulations in a montane stream. *Freshwater Biology*, *27*(2), 169–176. https://doi.org/10.1111/j.1365-2427.1992.tb00531.x

Rose, L. A., Karwan, D. L., & Aufdenkampe, A. K. (2018). Sediment fingerprinting suggests differential suspended particulate matter formation and transport processes across hydrologic regimes. *Journal of Geophysical Research: Biogeosciences*, *123*, 1213–1229. https://doi.org/10.1002/2017JG004210

Saffman, P. G. (1965). Lift on a small sphere in a slow shear flow. *Journal of Fluid Mechanics*, *22*, 385. https://doi.org/10.1017/s0022112065000824

Salant, N. L., Hassan, M. A., & Alonso, C. V. (2008). Suspended sediment dynamics at high and low storm flows in two small watersheds. *Hydrological Processes*, *22*(11), 1573–1587. https://doi.org/10.1002/hyp.6743

Shanley, J. B., Alisa Mast, M., Campbell, D. H., Aiken, G. R., Krabbenhoft, D. P., Hunt, R. J., et al. (2008). Comparison of total mercury and methylmercury cycling at five sites using the small watershed approach. *Environmental Pollution*, *154*(1), 143–154. https://doi.org/10.1016/j.envpol.2007.12.031

Skalak, K., & Pizzuto, J. (2010). The distribution and residence time of suspended sediment stored within the channel margins of a gravel-bed bedrock river. *Earth Surface Processes and Landforms*, *35*(4), 435–446. https://doi.org/10.1002/esp.1926

Sutfin, N. A., Wohl, E. E., & Dwire, K. A. (2016). Banking carbon: A review of organic carbon storage and physical factors influencing retention in floodplains and riparian ecosystems. *Earth Surface Processes and Landforms*, *41*(1), 38–60. https://doi.org/10.1002/esp.3857

Tank, J. L., Rosi-Marshall, E. J., Griffiths, N. A., Entrekin, S. A., & Stephen, M. L. (2010). A review of allochthonous organic matter dynamics and metabolism in streams. *Journal of the North American Benthological Society*, *29*(1), 118–146. https://doi.org/10.1899/08-170.1

Underwood, J. W., Renshaw, C. E., Magilligan, F. J., Dade, W. B., & Landis, J. D. (2015). Joint isotopic mass balance: A novel approach to quantifying channel bed to channel margins sediment transfer during storm events. *Earth Surface Processes and Landforms*, *40*(12), 1563–1573. https://doi.org/10.1002/esp.3734

USGS. (1982). *Guidelines for determining flood flow frequency*. Reston, VA: U.S. Geological Survey.

Vannote, R. L., Minshall, G. W., Cummins, K. W., Sedell, J. R., & Cushing, C. E. (1980). River continuum concept. *Canadian Journal of Fisheries and Aquatic Sciences*, *37*(1), b130–137. https://doi.org/10.1139/f80-017

Vorosmarty, C. J., Meybeck, M., Fekete, B., Sharma, K., Green, P., & Syvitski, J. P. M. (2003). Anthropogenic sediment retention: Major global impact from registered river impoundments. *Global and Planetary Change*, *39*(1–2), 169–190. https://doi.org/10.1016/s0921-8181(03)00023-7

Wagener, S. M., Oswood, M. W., & Schimel, J. P. (1998). Rivers and soils: Parallels in carbon and nutrient processing. *BioScience*, *48*(2), 104–108. https://doi.org/10.2307/1313135

Wallace, J. B., Whiles, M. R., Eggert, S., Cuffney, T. F., & Lugthart, G. J. (1995). Long-term dynamics of coarse particulate organic matter in three Appalachian mountain streams. *Journal of the North American Benthological Society*, *14*(2), 217–232. https://doi.org/10.2307/1467775

Walling, D. E. (2013). The evolution of sediment source fingerprinting investigations in fluvial systems. *Journal of Soils and Sediments*, *13*(10), 1658–1675. https://doi.org/10.1007/s11368-013-0767-2

Walling, D. E., He, Q., & Nicholas, A. P. (1996). Floodplains as suspended sediment sinks. In M. G.Anderson, D. E.Walling, & P. D.Bates (Eds.), *Floodplain processes* (pp. 399–440). New York, NY: John Wiley & Sons.

Walling, D. E., Schuller, P., Zhang, Y., & Iroume, A. (2009). Extending the timescale for using beryllium 7 measurements to document soil redistribution by erosion. *Water Resources Research*, *45*, W02418. https://doi.org/10.1029/2008WR007143

Walter, R. C., & Merritts, D. J. (2008). Natural streams and the legacy of water-powered mills. *Science*, *319*(5861), 299–304. https://doi.org/10.1126/science.1151716

Wang, X., Bao, Z. D., Lin, C. J., Yuan, W., & Feng, X. B. (2016). Assessment of global mercury deposition through litterfall. *Environmental Science & Technology*, *50*(16), 8548–8557. https://doi.org/10.1021/acs.est.5b06351

Webb, M., Barker, P. A., Wynn, P. M., Heiri, O., van Hardenbroek, M., Pick, F., et al. (2016). Interpretation and application of carbon isotope ratios in freshwater diatom silica. *Journal of Quaternary Science*, *31*(4), 300–309. https://doi.org/10.1002/jqs.2837

Webster, J. R., Wallace, J. B., & Benfield, E. F. (1995). Organics processes in streams of the eastern United States. In C. E.Cushing, G. W.Minshall, & K. W.Cummins (Eds.), *River and stream ecosystems* (pp. 103–164). Amsterdam: Elsevier Science.

Whiting, P. J., Matisoff, G., & Fornes, W. (2005). Suspended sediment sources and transport distances in the Yellowstone River basin. *Geological Society of America Bulletin*, *117*(3–4), 515–529. https://doi.org/10.1130/b25623.1

Wohl, E., Dwire, K., Sutfin, N., Polvi, L., & Bazan, R. (2012). Mechanisms of carbon storage in mountainous headwater rivers. *Nature Communications*, *3*, 1263. https://doi.org/10.1038/ncomms2274

Wolman, M. G., & Miller, J. P. (1960). Magnitude and frequency of forces in geomorphic processes. *The Journal of Geology*, *68*(1), 54–74. https://doi.org/10.1086/626637

Xia, R. J. (1997). Relation between mean and maximum velocities in a natural river. *Journal of Hydraulic Engineering-ASCE*, *123*(8), 720–723. https://doi.org/10.1061/(asce)0733-9429(1997)123:8(720)

Zhang, X., Walling, D. E., Yang, Q., He, X., Wen, Z., Qi, Y., & Feng, M. (2006). Cs-137 budget during the period of 1960s in a small drainage basin on the Loess Plateau of China. *Journal of Environmental Radioactivity*, *86*(1), 78–91. https://doi.org/10.1016/j.jenvrad.2005.07.007

Reference From the Supporting Information

Baskaran, M., & Santschi, P. H. (1993). The role of particles and colloids in the transport of radionuclides in coastal environments of Texas. *Marine Chemistry*, *43*(1–4), 95–114. https://doi.org/10.1016/0304-4203(93)90218-d